

Citation for published version:

K. Hussain and R. López-Valcarce, "Joint Precoder and Window Design for OFDM Sidelobe Suppression," in *IEEE Communications Letters*, vol. 26, no. 12, pp. 3044-3048, Dec. 2022, doi: 10.1109/LCOMM.2022.3203521.

Peer reviewed version

Link to published version: [10.1109/LCOMM.2022.3203521](https://doi.org/10.1109/LCOMM.2022.3203521)

General rights:

© 2022 IEEE. Personal use of this material is permitted. Permission from IEEE must be obtained for all other uses, in any current or future media, including reprinting/republishing this material for advertising or promotional purposes, creating new collective works, for resale or redistribution to servers or lists, or reuse of any copyrighted component of this work in other works.

Joint Precoder and Window Design for OFDM Sidelobe Suppression

Khawar Hussain, *Member, IEEE*, and Roberto López-Valcarce^{id}, *Senior Member, IEEE*

Abstract—Spectral precoding and windowing are two effective approaches to reduce out-of-band radiation (OBR) in multicarrier systems. Their performance comes at the price of reduced throughput and additional computational complexity, so there is strong motivation for simultaneously using both techniques. We present a novel design that jointly optimizes the precoder and window coefficients to minimize radiated power within a user-selectable frequency region. Results show that the proposed design achieves a better OBR/throughput/complexity tradeoff than either of these individual techniques separately.

Index Terms—OFDM, out-of-band radiation, sidelobe suppression, windowing, spectral precoding.

I. INTRODUCTION

DUE to its inherent advantages, orthogonal frequency division multiplexing (OFDM) has established itself as the most popular multicarrier modulation scheme: it is spectrally efficient, robust against frequency-selective fading thanks to the cyclic prefix (CP), and well matched to multiple-input multiple-output (MIMO) operation [1]. Nevertheless, it has some drawbacks, including large spectrum sidelobes which cause high out-of-band radiation (OBR). To alleviate this issue, many techniques have been proposed, which can be broadly categorized as *frequency-domain* and *time-domain* methods.

Frequency-domain techniques suitably modify the samples at the input of the inverse fast Fourier transform (IFFT). Deactivating subcarriers near the band edges to shape the spectrum is simple but very inefficient, due to the high subcarrier sidelobes. Multiple choice sequence techniques [2], [3] require the transmission of side information with each symbol, increasing system overhead. Data-dependent techniques, such as constellation expansion [4] or subcarrier weighting [5], [6], are computationally expensive, as they require solving an optimization problem per OFDM symbol.

Spectral precoding is another frequency-domain approach to mitigate OBR, by which the transmitted sequence is computed as a linear combination of the data [7], [8], [9], [10], [11]. In general, precoding introduces distortion, so appropriate decoding is required at the receiver to avoid error rate degradation. If the precoding matrix has orthonormal columns, its effect can be easily inverted at the receiver without noise enhancement [9], [10], [11]. Nevertheless, orthogonal precoding (OP) generally suffers from high computational

complexity. On the other hand, active interference cancellation (AIC) methods, which can be seen as a particular case of spectral precoding, use some reserved subcarriers for OBR reduction without altering the data subcarriers. Thus, AIC is transparent to the receiver, which merely discards the cancellation subcarriers [12], [13]. The complexity of AIC methods is significantly lower than that of OP, but at the expense of worse OBR performance. In both cases, additional subcarriers are required, with the corresponding impact on throughput.

Time-domain schemes modify the samples at the IFFT output. Standard filtering [14] is simple, but usually requires filters with long impulse responses, which decreases the effective guard interval of OFDM symbols. Data-dependent techniques like adaptive symbol transition [15] incur additional complexity, similarly to their frequency-domain counterparts. The typical rectangular pulse in CP-OFDM can be replaced by a pulse (or *window*) with soft edges, resulting in much sharper sidelobe decay in the frequency domain, a technique known as weighted overlap-add (WOLA) [16] or windowed OFDM (W-OFDM) [17]. The complexity of W-OFDM is low as compared to other OFDM-derived waveforms [18], but at the price of reduced efficiency due to the need to extend the symbol length. Different window functions are discussed in [19]. Among them, the raised cosine (RC) window is commonly used for its good performance and straightforward implementation [20]. The window can also be specifically tailored to minimize OBR over a desired range of frequencies [21].

Time- and frequency-domain approaches have their own advantages and drawbacks, and their tradeoffs involving OBR reduction, computational complexity, and throughput efficiency need not be the same. Such tradeoffs should improve by simultaneously acting in both domains; for example, a spectral precoder could be designed for a given window, as in [22]. Our goal is to further improve on such approach by *jointly* optimizing both precoder and window coefficients. Further differences between our design and [22] include: (i) we allow to target arbitrary frequency ranges by leveraging the design from [21] rather than using notch frequencies; (ii) we allow redundant spectral precoders, establishing the overall throughput efficiency once this redundancy is taken into account together with the symbol length extension due to windowing. The benefits of the proposed joint design, which is data-independent and can be computed offline, are illustrated for two particular precoding techniques which do not affect the bit error rate, namely OP and AIC.

II. SYSTEM MODEL

Consider an OFDM signal generated with an IFFT of size N . Let $\mathcal{K} = \{k_1, k_2, \dots, k_K\}$ denote the set of active

Manuscript received 17 August 2022; accepted 29 August 2022. This work was funded by MCIN/AEI/10.13039/501100011033 and FEDER “Una manera de hacer Europa” under project RODIN (PID2019-105717RB-C21/C22) and fellowship BES-2017-080305. The associate editor coordinating the review of this letter and approving it for publication was C. Huang. (*Corresponding author: Roberto López-Valcarce.*)

The authors are with the atlantTic Research Center, Universidade de Vigo, 36310 Vigo, Spain (e-mail: khawar@gts.uvigo.es; valcarce@gts.uvigo.es).

Digital Object Identifier 10.1109/LCOMM.2022.3203521

92 subcarriers, and $x_k^{(m)}$ be the data modulated on the k -th
 93 subcarrier in the m -th symbol. The baseband samples of the
 94 multicarrier signal are then given by

$$95 \quad s[n] = \sum_{m=-\infty}^{\infty} \sum_{k \in \mathcal{K}} x_k^{(m)} h_P[n - mL] e^{\frac{2\pi}{N} k(n - mL)}, \quad (1)$$

96 where L is the hop size in samples, and $h_P[n]$ is
 97 the shaping pulse, with Fourier transform $H_P(e^{j\omega}) =$
 98 $\sum_{n=-\infty}^{\infty} h_P[n] e^{-j\omega n}$. The analog baseband signal is

$$99 \quad s(t) = \sum_{n=-\infty}^{\infty} s[n] h_I(t - nT_s), \quad (2)$$

100 where T_s is the sampling interval, and $h_I(t)$ is the
 101 impulse response of the interpolation filter in the Digital-
 102 to-Analog Converter (DAC), with transform $H_I(f) =$
 103 $\int_{-\infty}^{\infty} h_I(t) e^{-j2\pi ft} dt$. With $\Delta_f = \frac{1}{NT_s}$ the subcarrier spacing,
 104 let us define

$$105 \quad \phi_k(f) \triangleq H_P^* \left(e^{j2\pi(f - k\Delta_f)T_s} \right), \quad (3)$$

$$106 \quad \phi(f) \triangleq [\phi_{k_1}(f) \quad \phi_{k_2}(f) \quad \cdots \quad \phi_{k_K}(f)]^T. \quad (4)$$

107 The pulse $h_P[n]$ extends from $n = 0$ to $n = L + Q - 1$, so that
 108 the first and the last Q samples of any consecutive symbols
 109 overlap. The central samples of $h_P[n]$ are fixed to 1 to avoid
 110 distortion at the receiver: $h_P[n] = 1$ for $Q \leq n \leq L - 1$;
 111 whereas the edge samples $h_P[n]$ for $n = 0, 1, \dots, Q - 1$ and
 112 $n = L, L + 1, \dots, L + Q - 1$ are to be designed. The
 113 gradual transition from 0 to 1 results in a sharper PSD.
 114 On the other hand, the effective CP length is reduced to
 115 $N_{CP} = L - N - Q$ samples due to the Q -sample overlap
 116 between consecutive symbols; therefore, for a given effective
 117 CP length (determined by the maximum expected length of the
 118 channel impulse response), windowing results in a throughput
 119 efficiency reduction by a factor $\frac{N + N_{CP}}{N + N_{CP} + Q}$.

120 III. POWER SPECTRAL DENSITY

121 Let $\mathbf{d}_m \in \mathbb{C}^D$, with $D \leq K$, be the data sequence to
 122 transmit. Each entry of \mathbf{d}_m is independently drawn from an
 123 M -ary constellation \mathcal{C} with zero mean and unit variance,
 124 so that $\mathbb{E}\{\mathbf{d}_m\} = \mathbf{0}$ and $\mathbb{E}\{\mathbf{d}_m \mathbf{d}_m^H\} = \delta_{mm'} \mathbf{I}_D$. Thus,
 125 $R = K - D$ is the precoder redundancy. The vector of samples
 126 in the m -th block is denoted as

$$127 \quad \mathbf{x}_m \triangleq [x_{k_1}^{(m)} \quad x_{k_2}^{(m)} \quad \cdots \quad x_{k_K}^{(m)}]^T. \quad (5)$$

128 We consider linear memoryless precoding, for which $\{\mathbf{x}_m\}$ is
 129 generated from $\{\mathbf{d}_m\}$ as

$$130 \quad \mathbf{x}_m = \mathbf{G} \mathbf{d}_m, \quad (6)$$

131 where $\mathbf{G} \in \mathbb{C}^{K \times D}$ is the precoding matrix. Then, as shown
 132 in [23], the power spectral density (PSD) of $s(t)$ is given by

$$133 \quad S_s(f) = \frac{|H_I(f)|^2}{LT_s} \phi^H(f) \mathbf{G} \mathbf{G}^H \phi(f). \quad (7)$$

134 Note that $\phi(f)$ in (4) can be rewritten as $\phi(f) = \mathbf{M}(f) \mathbf{h}$,
 135 where $\mathbf{M}(f) \in \mathbb{C}^{K \times (L+Q)}$ is given entrywise by

$$136 \quad [\mathbf{M}(f)]_{pq} = e^{j2\pi(q-1)(f - k_p \Delta_f)}, \quad \begin{cases} 1 \leq p \leq K, \\ 1 \leq q \leq L + Q, \end{cases} \quad (8)$$

and $\mathbf{h} \in \mathbb{C}^{L+Q}$ comprises the (conjugated) pulse samples: 137

$$138 \quad \mathbf{h} \triangleq [h^*[0] \quad h^*[1] \quad \cdots \quad h^*[L + Q - 1]]^T. \quad (9)$$

Thus, $S_s(f)$ in (7) can be rewritten in terms of \mathbf{G} and \mathbf{h} as 139

$$140 \quad S_s(f) = \frac{|H_I(f)|^2}{LT_s} \mathbf{h}^H \mathbf{M}^H(f) \mathbf{G} \mathbf{G}^H \mathbf{M}(f) \mathbf{h}. \quad (10)$$

141 IV. JOINT PRECODER AND WINDOW DESIGN

142 Let $W(f) \geq 0$ be a weighting function, giving emphasis
 143 to those frequencies over which PSD reduction is important.
 144 Then, the weighted power, which quantifies OBR, is given by

$$145 \quad \mathcal{P}_W = \int_{-\infty}^{\infty} W(f) S_s(f) df. \quad (11)$$

146 The goal is to minimize \mathcal{P}_W with respect to the pulse \mathbf{h} and
 147 precoder \mathbf{G} . This general problem can be stated as

$$148 \quad \min_{\mathbf{h}, \mathbf{G}} \mathcal{P}_W(\mathbf{h}, \mathbf{G}) \quad \text{s. to} \quad \begin{cases} h[n] = 1, & Q \leq n \leq L - 1, \\ \text{structural constraint on } \mathbf{G}. \end{cases} \quad (12)$$

149 The second constraint in (12) depends on the particular pre-
 150 coder structure (e.g., OP or AIC) as discussed below.

151 Problem (12) is nonconvex in general. However, if either
 152 \mathbf{h} or \mathbf{G} is fixed, the corresponding subproblem becomes
 153 manageable. Thus, we propose to cyclically minimize \mathcal{P}_W
 154 with respect to these parameters (pulse and precoder).

155 A. Optimal Window for a Given Precoder

156 For fixed \mathbf{G} , the weighted power in (11) becomes $\mathcal{P}_W =$
 157 $\mathbf{h}^H \mathbf{Z}(\mathbf{G}) \mathbf{h}$, where $\mathbf{Z}(\mathbf{G}) \in \mathbb{C}^{(L+Q) \times (L+Q)}$ is given by

$$158 \quad \mathbf{Z}(\mathbf{G}) \triangleq \int_{-\infty}^{\infty} W(f) \frac{|H_I(f)|^2}{LT_s} \mathbf{M}^H(f) \mathbf{G} \mathbf{G}^H \mathbf{M}(f) df, \quad (13)$$

160 which is Hermitian positive (semi-)definite. Then the following
 161 convex subproblem is obtained:

$$162 \quad \min_{\mathbf{h}} \mathbf{h}^H \mathbf{Z}(\mathbf{G}) \mathbf{h} \quad \text{s. to} \quad \mathbf{J}^H \mathbf{h} = \mathbf{1}, \quad (14)$$

163 where $\mathbf{J} \in \mathbb{C}^{(L+Q) \times (L+Q)}$ comprises columns $Q + 1$ through
 164 L of \mathbf{I}_{L+Q} , and $\mathbf{1} \in \mathbb{C}^{L-Q}$ is the all-ones vector. The solution
 165 to (14) can be readily found in closed form: letting $\tilde{\mathbf{J}} \in$
 166 $\mathbb{C}^{(L+Q) \times 2Q}$ comprise columns 1 through Q and $L + 1$ through
 167 $L + Q$ of \mathbf{I}_{L+Q} , then $\tilde{\mathbf{J}}^H \mathbf{h}$ contains the edge samples of \mathbf{h} ,
 168 given by $\tilde{\mathbf{J}}^H \mathbf{h} = -(\tilde{\mathbf{J}}^H \mathbf{Z}(\mathbf{G}) \tilde{\mathbf{J}})^{-1} \tilde{\mathbf{J}}^H \mathbf{Z}(\mathbf{G}) \mathbf{J} \mathbf{1}$.

169 B. Optimal Precoder for a Given Window

170 The PSD from (10) can be rewritten as

$$171 \quad S_s(f) = \text{tr}\{\mathbf{G}^H \Phi(f; \mathbf{h}) \mathbf{G}\}, \quad (15)$$

172 where $\Phi(f; \mathbf{h}) \triangleq \frac{|H_I(f)|^2}{LT_s} \mathbf{M}(f) \mathbf{h} \mathbf{h}^H \mathbf{M}^H(f)$. Thus, letting
 173 $\mathbf{A}_W(\mathbf{h}) \triangleq \int_{-\infty}^{\infty} W(f) \Phi(f; \mathbf{h}) df$, \mathcal{P}_W in (11) becomes

$$174 \quad \mathcal{P}_W = \text{tr}\{\mathbf{G}^H \mathbf{A}_W(\mathbf{h}) \mathbf{G}\}. \quad (16)$$

1) *Orthogonal Precoder*: With OP, the structural constraint on the precoder reads as $\mathbf{G}^H \mathbf{G} = \mathbf{I}_D$, yielding

$$\min_{\mathbf{G}} \text{tr}\{\mathbf{G}^H \mathbf{A}_W(\mathbf{h}) \mathbf{G}\} \quad \text{s. to } \mathbf{G}^H \mathbf{G} = \mathbf{I}_D, \quad (17)$$

whose solution \mathbf{G} comprises the eigenvectors of $\mathbf{A}_W(\mathbf{h})$ corresponding to the D smallest eigenvalues.

2) *AIC Precoder*: The data vector \mathbf{d}_m is directly mapped to D of the K active subcarriers, whereas the remaining $R = K - D$ subcarriers are used for cancellation. Let $\mathbf{S} \in \mathbb{C}^{K \times D}$ comprise the D columns of \mathbf{I}_K corresponding to the indices of active subcarriers to which the data is directly mapped, and let $\mathbf{T} \in \mathbb{C}^{K \times (K-D)}$ comprise the remaining $K - D$ columns of \mathbf{I}_K . Then the structural constraint on the AIC precoder is $\mathbf{G} = \mathbf{S} + \mathbf{T}\Theta$, where \mathbf{S}, \mathbf{T} are fixed whereas $\Theta \in \mathbb{C}^{(K-D) \times D}$ is a free parameter. Minimizing $\mathcal{P}_W = \text{tr}\{(\mathbf{S} + \mathbf{T}\Theta)^H \mathbf{A}_W(\mathbf{h})(\mathbf{S} + \mathbf{T}\Theta)\}$ w.r.t. Θ is a convex quadratic problem with solution $\Theta = -(\mathbf{T}^H \mathbf{A}_W(\mathbf{h}) \mathbf{T})^{-1} \mathbf{T} \mathbf{A}_W(\mathbf{h}) \mathbf{S}$. However, this may result in too much power being allocated to cancellation subcarriers, resulting in undesirably large PSD peaks. To control the size of these peaks, a regularization term can be introduced, leading to the following subproblem:

$$\min_{\Theta} \text{tr}\{(\mathbf{S} + \mathbf{T}\Theta)^H \mathbf{A}_W(\mathbf{h})(\mathbf{S} + \mathbf{T}\Theta)\} + \gamma \|\Theta\|_F^2, \quad (18)$$

where larger values of the regularization parameter $\gamma \geq 0$ will result in lower spectral peaks. The solution to (18) is given by $\Theta = -(\mathbf{T}^H \mathbf{A}_W(\mathbf{h}) \mathbf{T} + \gamma \mathbf{I}_R)^{-1} \mathbf{T} \mathbf{A}_W(\mathbf{h}) \mathbf{S}$.

C. Cyclic Optimization

To obtain an approximate solution to (12), we first initialize \mathbf{h}_0 as an RC window. Then, for $k \geq 1$, we solve:

$$\text{OP: } \mathbf{G}_k = \arg \min_{\mathbf{G}} \mathcal{P}_W(\mathbf{h}_{k-1}, \mathbf{G})$$

$$\text{s. to } \mathbf{G}^H \mathbf{G} = \mathbf{I}_D \quad (19)$$

$$\text{AIC: } \mathbf{G}_k = \arg \min_{\mathbf{G}} \mathcal{P}_W(\mathbf{h}_{k-1}, \mathbf{G}) + \gamma \|\Theta\|_F^2$$

$$\text{s. to } \mathbf{G} = \mathbf{S} + \mathbf{T}\Theta \quad (20)$$

$$\text{OP \& AIC: } \mathbf{h}_k = \arg \min_{\mathbf{h}} \mathcal{P}_W(\mathbf{h}, \mathbf{G}_k)$$

$$\text{s. to } \mathbf{J}^H \mathbf{h} = \mathbf{1}. \quad (21)$$

Note that the sequence of objective values $\mathcal{P}_W(\mathbf{h}_k, \mathbf{G}_k)$ for OP, or $\mathcal{P}_W(\mathbf{h}_k, \mathbf{G}_k) + \gamma \|\Theta_k\|_F^2$ for AIC, is non-increasing and bounded below, so it must be convergent. Although there is no guarantee that the global optimum of (12) is found, simulation results validate the good performance of the proposed scheme.

V. RECEIVER OPERATION, EFFICIENCY, AND COMPLEXITY

At the receiver end, after synchronization, the CP and the Q overlapping samples between consecutive blocks are removed. After an N -point FFT and equalization, the vector $\mathbf{r} \in \mathbb{C}^K$ with the samples of active subcarriers is obtained. With OP, data can be estimated as $\text{DEC}\{\mathbf{G}^H \mathbf{r}\}$, where $\text{DEC}\{\cdot\}$ is an entrywise operator returning, for each entry, the closest symbol in the constellation; since \mathbf{G} has orthonormal columns, noise enhancement is avoided. On the other hand, AIC is transparent to the receiver: data can be estimated as $\text{DEC}\{\mathbf{S}^H \mathbf{r}\}$, i.e., cancellation subcarriers are simply discarded.

Each OFDM block, carrying D data symbols, is sent every LT_s seconds, so that the bit rate is $R_b = \frac{D}{LT_s} = \frac{(K-R) \log_2 M}{(N+N_{\text{CP}}+Q)T_s}$ bits/s. For the same effective CP length N_{CP} , the baseline is given by a system with no precoding ($R = 0$) and without windowing ($Q = 0$), whose corresponding bit rate is $R_{b,\text{ref}} = \frac{K \log_2 M}{(N+N_{\text{CP}})T_s}$ bits/s. Hence, the metric for throughput efficiency is

$$\eta = \frac{R_b}{R_{b,\text{ref}}} = \frac{1 - R/K}{1 + Q/(N_{\text{CP}} + N)}, \quad (22)$$

which depends on the relative precoder redundancy $\frac{R}{K}$ and the relative window redundancy $\frac{Q}{N_{\text{CP}} + N}$. Thus, a given efficiency η can be achieved with different (R, Q) values, by using longer windows with fewer redundant subcarriers, or vice versa.

The proposed design is data-independent, so it can be computed offline. Regarding online complexity, windowing takes $2Q$ complex multiplications per OFDM symbol (cm/symb) at the transmitter, whereas no additional complexity is incurred at the receiver; with respect to the precoder, one has:

- **OP.** The online complexity at each of transmitter and receiver is $K(K - R)$ cm/symb, if multiplication by \mathbf{G} or \mathbf{G}^H is implemented directly, but it becomes $R(2K - R)$ cm/symb with Clarkson's reduced complexity approach [24], which will be assumed in the sequel. With this, the total complexity including windowing and precoding is $2R(2K - R) + 2Q$ cm/symb.
- **AIC.** At the transmitter, AIC requires $R(K - R)$ cm/symb. At the receiver end, the R cancellation subcarriers are just discarded, with no additional complexity. The total complexity is thus $R(K - R) + 2Q$ cm/symb.

VI. RESULTS

We study the performance of the proposed *joint precoder and window* (JPW) design in a CP-OFDM system with IFFT size $N = 256$ and CP length $N_{\text{CP}} = N/4$. The DAC filter is lowpass with $H_1(f) = 1$ for $|f| \leq \frac{1}{2T_s}$ and zero otherwise. There are $K = 65$ active subcarriers, located symmetrically about the carrier frequency. The weighting function is $W(f) = 1, \forall \left\{ \frac{1}{8T_s} + \frac{\Delta_f}{2} \leq |f| \leq \frac{1}{2T_s} \right\}$, and zero otherwise.

A. Windowing and Orthogonal Precoding

For a given efficiency η , JPW provides the flexibility to trade off complexity and OBR reduction by choosing R and Q . Fig. 1 shows the PSD obtained by JPW with orthogonal precoding (JPW-OP), along with that of standard CP-OFDM with 5 null subcarriers at each band edge, for the above system parameters and fixing $\eta = 84.6\%$. Note that $(R, Q) = (10, 0)$ corresponds to orthogonal precoding with rectangular pulses, whereas $(R, Q) = (0, 58)$ reduces to the optimal window design from [21] with no precoding. It is seen that windowing, by itself, is unable to provide a fast rolloff at the passband edge; an orthogonal precoder, without windowing, performs much better in this regard, but the associated online complexity is significantly higher. The tradeoff provided by JPW-OP is clearly seen in Fig. 1, and also in Table I. For $(R, Q) = (8, 12)$, JPW-OP provides a 4.3-dB OBR improvement with

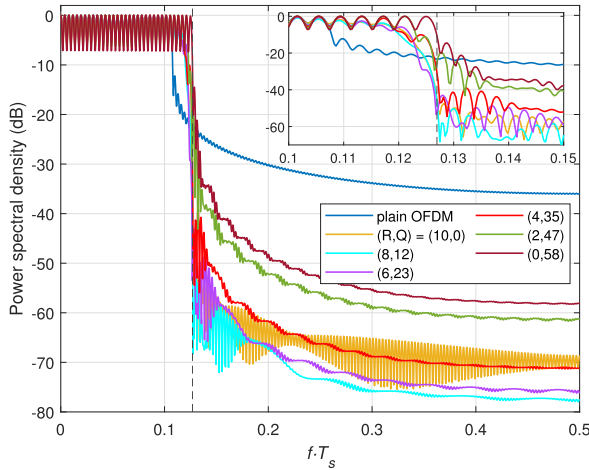


Fig. 1. PSD of the proposed JPW-OP design for different (R, Q) pairs. $\eta = 84.6\%$, $N = 256$, $N_{CP} = N/4$, $K = 65$.

TABLE I

ONLINE COMPLEXITY AND OBR (RELATIVE TO THAT OF PLAIN CP-OFDM WITH 10 NULL SUBCARRIERS) OF JPW-OP AND RC-OP. $\eta = 84.6\%$

(R, Q)	(10, 0)	(8, 12)	(6, 23)	(4, 35)	(2, 47)	(0, 58)
cm/symb	2400 100%	1976 82.3%	1534 63.9%	1078 44.9%	606 25.2%	116 4.8%
OBR, dB						
JPW-OP	-31.8	-36.1	-31.3	-24.1	-10.6	-3.9
RC-OP	-31.8	-30.6	-28.9	-22.8	-9.0	-2.8

276 respect to the standard orthogonal precoder, with 82.3% of its
 277 complexity. With $(R, Q) = (6, 23)$, complexity can be reduced
 278 to 63.9%, with just a small OBR degradation of 0.5 dB.

279 Table I also shows the results for a simplified design in
 280 which the window is fixed to an RC pulse, and then the
 281 orthogonal precoder is optimized for this fixed window, as pro-
 282 posed in [22]. This approach, termed ‘‘RC-OP’’, corresponds to
 283 performing (19) for iteration $k = 1$ of the JPW-OP design, and
 284 then stopping. (We denote ‘‘RC-AIC’’ the analogous strategy
 285 for AIC precoders). Whereas JPW-OP and RC-OP have the
 286 same online complexity for a given (R, Q) pair, it is seen
 287 that jointly optimizing the precoder and the pulse improves
 288 OBR performance, *e.g.*, by 5.5 dB for $(R, Q) = (8, 12)$.
 289 Nevertheless, the RC-OP design may be attractive in dynamic
 290 spectrum access scenarios requiring frequent recomputation of
 291 precoder and window parameters due to the varying availabil-
 292 ity of spectral subbands.

293 B. Windowing and AIC Precoding

294 In addition to being transparent to the receiver, AIC is
 295 computationally much simpler than orthogonal precoding.
 296 Thus, the online complexity of JPW with AIC precoding
 297 (JPW-AIC) is significantly lower than that of JPW-OP. Fig. 2
 298 shows the corresponding PSDs for $\eta = 84.6\%$. In each case,
 299 half of the R cancellation subcarriers are placed at each of the
 300 passband edges, and the regularization parameter γ is adjusted
 301 to prevent spectral peaks above 2 dB. It is seen that both
 302 AIC precoding without windowing, *i.e.*, $(R, Q) = (10, 0)$,
 303 and windowing without precoding, *i.e.*, $(R, Q) = (0, 58)$,
 304 present serious limitations in terms of sidelobe suppression.
 305 By suitably choosing (R, Q) , performance can be significantly

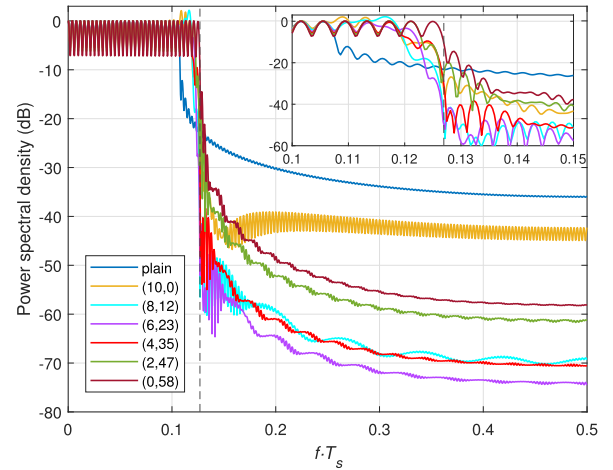


Fig. 2. PSD of JPW-AIC for different (R, Q) pairs. $\eta = 84.6\%$. Spectral peak is limited to 2 dB. $N = 256$, $N_{CP} = N/4$, $K = 65$.

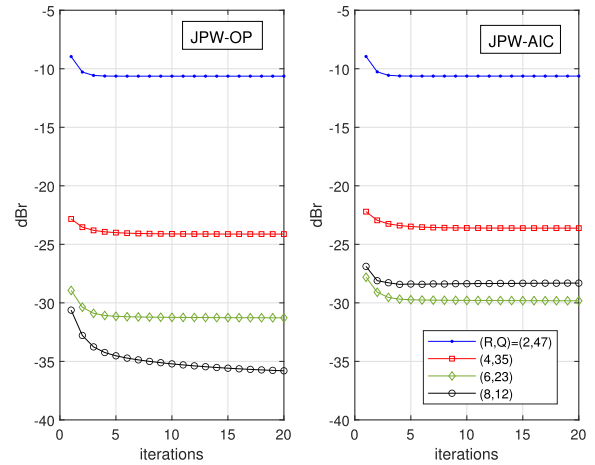


Fig. 3. Convergence of the proposed designs in terms of OBR in the setting of Figs. 1 and 2.

TABLE II

ONLINE COMPLEXITY AND OBR (RELATIVE TO THAT OF PLAIN CP-OFDM WITH 10 NULL SUBCARRIERS) OF JPW-AIC AND RC-AIC. $\eta = 84.6\%$, SPECTRAL PEAK ≤ 2 dB

(R, Q)	(10, 0)	(8, 12)	(6, 23)	(4, 35)	(2, 47)	(0, 58)
cm/symb	550 100%	480 87.3%	400 72.7%	314 57%	220 40%	116 21%
OBR, dB						
JPW-AIC	-9.9	-28.3	-29.8	-23.6	-10.6	-3.9
RC-AIC	-9.9	-26.5	-27.8	-22.2	-9.0	-2.8

306 improved, as seen in Fig. 2 and Table II. As a side benefit,
 307 for $R \leq 6$, the joint use of windowing and precoding turns out
 308 to avoid spectral peaks altogether in this case. Fig. 3 shows
 309 the convergence of the cyclic scheme (19)-(21) in this setting.

310 Interestingly, JPW-AIC may be able to provide OBR reduc-
 311 tion levels comparable to those obtained with the standard (*i.e.*,
 312 no windowing) orthogonal precoder, with much less online
 313 complexity. From Tables I and II, it is seen that for the same
 314 efficiency ($\eta = 84.6\%$), JPW-AIC with $(R, Q) = (6, 23)$ per-
 315 forms only 2 dB worse than the standard orthogonal precoder,
 316 with just $\frac{400}{2400} = 16.7\%$ of the complexity (which is all placed
 317 at the transmitter). This is further illustrated in Table III, which
 318 shows the results obtained in this setting for two CP lengths
 319 ($N/4$ and $N/16$) and for different efficiency values, and where

TABLE III
ONLINE COMPLEXITY AND OBR (RELATIVE TO PLAIN OFDM WITH NULL SUBCARRIERS) OF DIFFERENT DESIGNS. $N = 256$, $K = 65$

η	90.8%		87.7%		84.6%		81.5%		78.5%	
$N_{CP} = N/4$	cm/symb	dBr	cm/symb	dBr	cm/symb	dBr	cm/symb	dBr	cm/symb	dBr
OP (R)	1488 (6)	-14.5	1952 (8)	-22.8	2400 (10)	-31.8	2832 (12)	-41.4	3248 (14)	-51.1
AIC (R)	354 (6)	-6.3	456 (8)	-7.9	550 (10)	-9.8	636 (12)	-11.5	714 (14)	-13.3
W-OFDM (Q)	33 (16)	-1.8	90 (45)	-3.2	116 (58)	-3.9	144 (72)	-4.7	176 (88)	-5.6
RC-OP (R, Q)	1030 (4,11)	-14.5	1510 (6,11)	-23.5	1976 (8,12)	-30.6	2424 (10,12)	-33.0	2858 (12,13)	-37.2
JPW-OP (R, Q)		-15.6		-24.6		-36.1		-47.1		-49.2
RC-AIC (R, Q)	266 (4,11)	-12.7	376 (6,11)	-20.9	400 (6,23)	-27.8	504 (8,24)	-31.1	530 (8,37)	-32.3
JPW-AIC (R, Q)		-14.2		-22.3		-29.8		-42.1		-50.8
$N_{CP} = N/16$	cm/symb	dBr	cm/symb	dBr	cm/symb	dBr	cm/symb	dBr	cm/symb	dBr
OP (R)	1488 (6)	-18.3	1952 (8)	-27.1	2400 (10)	-37.7	2832 (12)	-50.5	3248 (14)	-67.6
AIC (R)	354 (6)	-3.5	456 (8)	-4.5	550 (10)	-5.4	636 (12)	-6.9	714 (14)	-7.8
W-OFDM (Q)	56 (28)	-1.9	76 (38)	-2.4	98 (49)	-3.1	124 (62)	-3.9	150 (75)	-4.7
RC-OP (R, Q)	1026 (4,9)	-14.0	1508 (6,10)	-27.1	1528 (6,20)	-30.6	1994 (8,21)	-32.9	2442 (10,21)	-37.7
JPW-OP (R, Q)		-15.3		-29.0		-35.5		-46.0		-60.3
RC-AIC (R, Q)	262 (4,9)	-9.4	282 (4,19)	-14.5	394 (6,20)	-21.2	416 (6,31)	-30.4	440 (6,43)	-31.7
JPW-AIC (R, Q)		-11.1		-16.4		-23.3		-35.4		-42.2

we have picked the pair (R, Q) corresponding to the largest OBR reduction for JPW-OP and JPW-AIC in each case. For all AIC-based schemes, spectral peaks are kept below 2 dB.

VII. CONCLUSION

Energy efficiency is a critical aspect of wireless transceivers, and thus it is important to exploit all available tools at one's disposal to perform a given task with the lowest energy consumption. We have shown that, for multicarrier systems, the combination of spectral precoding and windowing has the potential to provide sidelobe suppression comparable to that of standard precoding while sustaining the same throughput, but with much less online complexity. The proposed design for jointly computing precoder and window coefficients can be run offline, and it can be flexibly adapted to emphasize suppression over a user-selectable frequency range.

REFERENCES

[1] Y. Li and G. Stüber, Eds., *Orthogonal Frequency Division Multiplexing for Wireless Communications*. Boston, MA, USA: Springer, 2006.
 [2] I. Cosovic and V. Janardhanam, "Sidelobe suppression in OFDM systems," in *Multi-Carrier Spread-Spectrum*, K. Fazel and S. Kaiser, Eds. Dordrecht, The Netherlands: Springer, 2006, pp. 473-482.
 [3] I. Cosovic and T. Mazzoni, "Suppression of sidelobes in OFDM systems by multiple-choice sequences," *Eur. Trans. Telecommun.*, vol. 17, no. 6, pp. 623-630, 2006.
 [4] S. Pagadarai, R. Rajbanshi, A. M. Wyglinski, and G. J. Minden, "Sidelobe suppression for OFDM-based cognitive radios using constellation expansion," in *Proc. IEEE Wireless Commun. Netw. Conf.*, Mar. 2008, pp. 888-893.
 [5] I. Cosovic, S. Brandes, and M. Schnell, "Subcarrier weighting: A method for sidelobe suppression in OFDM systems," *IEEE Commun. Lett.*, vol. 10, no. 6, pp. 444-446, Jun. 2006.
 [6] R. Kumar and A. Tyagi, "Extended subcarrier weighting for sidelobe suppression in OFDM based cognitive radio," *Wireless Pers. Commun.*, vol. 87, no. 3, pp. 779-796, Apr. 2016, doi: 10.1007/S11277-015-2623-8.
 [7] C.-D. Chung, "Spectrally precoded OFDM," *IEEE Trans. Commun.*, vol. 54, no. 12, pp. 2173-2185, Dec. 2006.
 [8] J. van der Beek, "Sculpting the multicarrier spectrum: A novel projection precoder," *IEEE Commun. Lett.*, vol. 13, no. 12, pp. 881-883, Dec. 2009.

[9] R. Xu and M. Chen, "A precoding scheme for DFT-based OFDM to suppress sidelobes," *IEEE Commun. Lett.*, vol. 13, no. 10, pp. 776-778, Oct. 2009.
 [10] M. Ma, X. Huang, B. Jiao, and Y. J. Guo, "Optimal orthogonal precoding for power leakage suppression in DFT-based systems," *IEEE Trans. Commun.*, vol. 59, no. 3, pp. 844-853, Mar. 2011.
 [11] R. Kumar, K. Hussain, and R. Lopez-Valcarce, "Mask-compliant orthogonal precoding for spectrally efficient OFDM," *IEEE Trans. Commun.*, vol. 69, no. 3, pp. 1990-2001, Mar. 2021.
 [12] S. Brandes, I. Cosovic, and M. Schnell, "Reduction of out-of-band radiation in OFDM systems by insertion of cancellation carriers," *IEEE Commun. Lett.*, vol. 10, no. 6, pp. 420-422, Jun. 2006.
 [13] J. F. Schmidt, S. Costas-Sanz, and R. Lopez-Valcarce, "Choose your subcarriers wisely: Active interference cancellation for cognitive OFDM," *IEEE J. Emerg. Sel. Topics Circuits Syst.*, vol. 3, no. 4, pp. 615-625, Dec. 2013.
 [14] M. Faulkner, "The effect of filtering on the performance of OFDM systems," *IEEE Trans. Veh. Technol.*, vol. 49, no. 5, pp. 1877-1884, Sep. 2000.
 [15] H. Mahmoud and H. Arslan, "Sidelobe suppression in OFDM-based spectrum sharing systems using adaptive symbol transition," *IEEE Commun. Lett.*, vol. 12, no. 2, pp. 133-135, Feb. 2008.
 [16] R. Zayani, Y. Medjahdi, H. Shaiek, and D. Roviras, "WOLA-OFDM: A potential candidate for asynchronous 5G," in *Proc. IEEE Global Commun. Conf. (GLOBECOM)*, Dec. 2016, pp. 1-5.
 [17] A. A. Zaidi et al., "Waveform and numerology to support 5G services and requirements," *IEEE Commun. Mag.*, vol. 54, no. 11, pp. 90-98, Nov. 2016.
 [18] S.-Y. Lien, S.-L. Shieh, Y. Huang, B. Su, Y.-L. Hsu, and H.-Y. Wei, "5G new radio: Waveform, frame structure, multiple access, and initial access," *IEEE Commun. Mag.*, vol. 55, no. 6, pp. 64-71, Jun. 2017.
 [19] B. Farhang-Boroujeny, "OFDM versus filter bank multicarrier," *IEEE Signal Process. Mag.*, vol. 28, no. 3, pp. 92-112, May 2011.
 [20] *Waveform Candidates*, document D. R1-162199, Qualcomm Inc., Busan, South Korea, Apr. 2016.
 [21] K. Hussain and R. Lopez-Valcarce, "Optimal window design for W-OFDM," in *Proc. IEEE Int. Conf. Acoust., Speech Signal Process. (ICASSP)*, May 2020, pp. 5275-5289.
 [22] T. Taheri, R. Nilsson, and J. van de Beek, "Hybrid spectral precoding/windowing for low-latency OFDM," in *Proc. IEEE 85th Veh. Technol. Conf. (VTC Spring)*, Jun. 2017, pp. 1-5.
 [23] R. Lopez-Valcarce, "General form of the power spectral density of multicarrier signals," *IEEE Commun. Lett.*, vol. 26, no. 8, pp. 1755-1759, Aug. 2022.
 [24] I. V. L. Clarkson, "Orthogonal precoding for sidelobe suppression in DFT-based systems using block reflectors," in *Proc. IEEE Int. Conf. Acoust., Speech Signal Process. (ICASSP)*, Mar. 2017, pp. 3709-3713.